Journal of the Mechanics and Physics of Solids 79 (2015) 1–20

Contents lists available at ScienceDirect

Journal of the Mechanics and Physics of Solids

journal homepage: www.elsevier.com/locate/jmps

Strain gradient plasticity modeling of the cyclic behavior of laminate microstructures

Stephan Wulfinghoff [a,*], Samuel Forest [b], Thomas Böhlke [a]

[a] Karlsruhe Institute of Technology (KIT), Institute of Engineering Mechanics (Continuum Mechanics), Kaiserstraße 12, 76131 Karlsruhe, Germany

[b] Mines ParisTech, Centre des Matériaux, CNRS UMR 7633 BP 87, 91003 Evry Cedex, France

ARTICLE INFO

Article history:
Received 24 September 2014
Received in revised form
17 December 2014
Accepted 9 February 2015
Available online 11 March 2015

Keywords:
Gradient plasticity
Non-smooth defect energy
Sub-differential
Regularization
Logarithmic defect energy

ABSTRACT

Two recently proposed Helmholtz free energy potentials including the full dislocation density tensor as an argument within the framework of strain gradient plasticity are used to predict the cyclic elastoplastic response of periodic laminate microstructures. First, a rank-one defect energy is considered, allowing for a size-effect on the overall yield strength of micro-heterogeneous materials. As a second candidate, a logarithmic defect energy is investigated, which is motivated by the work of Groma et al. (2003). The properties of the back-stress arising from both energies are investigated in the case of a laminate microstructure for which analytical as well as numerical solutions are derived. In this context, a new regularization technique for the numerical treatment of the rank-one potential is presented based on an incremental potential involving Lagrange multipliers. The results illustrate the effect of the two energies on the macroscopic size-dependent stress–strain response in monotonic and cyclic shear loading, as well as the arising pile-up distributions. Under cyclic loading, stress–strain hysteresis loops with inflections are predicted by both models. The logarithmic potential is shown to provide a continuum formulation of Asaro's type III kinematic hardening model. Experimental evidence in the literature of such loops with inflections in two-phased FFC alloys is provided, showing that the proposed strain gradient models reflect the occurrence of reversible plasticity phenomena under reverse loading.

1. Introduction

Many industrial projects require systematic and efficient methods in order to miniaturize systems and design new material micro-structures successfully. Therefore, there is an increasing need for micro-mechanical material models. In this context, size effects are of particular importance. These are not captured by classical plasticity theories which do not possess an internal length scale.

This deficiency has motivated the mechanical community to enhance the classical constitutive equations. In particular, additional microstructural information is taken into account. In most cases, the kinematical framework is extended by plastic strain gradients. This choice is motivated by the correlation between size effects and plastic inhomogeneity, experimentally observed and predicted by dislocation mechanics (Hall, 1951; Petch, 1953; Stölken and Evans, 1998; Xiang and Vlassak, 2006; Gruber et al., 2008; Groma et al., 2003; Mesarovic et al., 2010, 2015).

* Corresponding author.

http://dx.doi.org/10.1016/j.jmps.2015.02.008
0022-5096/

Plastic deformation gradients can be interpreted physically because they define geometrically necessary dislocations (GNDs, see Ashby, 1970). GNDs represent the effective (or net) Burgers vector of the underlying dislocation network. In other words, the presence of GNDs is associated with the incompatibility of the mesoscopic plastic distorsion.

Extending the kinematical plasticity framework by GNDs has a major advantage: it renders the introduction of additional field variables obsolete.[1] However, the geometrical description of GNDs is not unique. For example, they may be represented by scalar edge and screw densities. These are defined for each slip system and interact through constitutive models (e.g. Gurtin et al., 2007).

Alternatively, the kinematical extension may be based on the full dislocation density tensor (Nye, 1953; Kröner, 1958). In this case, the interaction is implicitly defined (although little is known about the accuracy of this approach). The advantage of this pragmatic approach is to limit the number of additional degrees of freedom introduced in the theory and in its computational treatment. The present contribution is based on formulations involving the full dislocation density tensor because they are amenable to intensive 3D finite element simulations, in contrast to GND density based models which are much more demanding in terms of degrees of freedom and specific interface conditions at grain boundaries. This is a restrictive approach from the physical point of view but it already contains essential physical features of strain gradient crystal plasticity as demonstrated for instance in the works by Cordero et al. (2012) and Wulfinghoff et al. (2013a). However several aspects of the proposed analysis are applicable to GND density based theories. Phenomenological formulations based on the introduction of the dislocation density tensor are known to give rise to a backstress associated with kinematic hardening, as derived from continuum thermodynamics (Steinmann, 1996; Forest, 2008).

The extension of the kinematical framework allows for the desired modification of the constitutive model. Often, new generalized stresses are introduced, which are conjugate to the additional kinematical quantities (i.e. the gradients) in the power of internal forces. This usually implies extra balance equations (and associated boundary conditions) in addition to the linear momentum balance.

The system of equations must be closed by new constitutive bulk and interface models. This may be achieved by modeling the impact of strain gradients on the bulk energy density, for example. Usually, this is related to a backstress, which appears as an additional term in the flow rule.

Physically, the introduction of additional energy density terms may be motivated by the incompleteness of the continuum theory. Clearly, the continuum description does not contain the full information on the discrete dislocation microstructure. In particular, single dislocations are not resolved. Instead, the continuum representation may be interpreted as a smoothed version of the real system, where information is lost deliberately. Clearly, there is no reason to assume that the total elastic energy of the continuum representation coincides with the elastic energy of the real system including discrete dislocations. This is due to the loss of information as a result of the smoothing procedure (Mesarovic et al., 2010). Additional energy terms in gradient plasticity may therefore be interpreted as an attempt to partially compensate the error in the continuum elastic energy. This is done by taking into account available kinematical information on the dislocation microstructure as additional argument of the energy.

The optimal form of the energy is subject of current research. Typical models often involve internal length scale parameters. These are normally assumed to be additional material constants (usually without further physical interpretation). Most applications are based on a pragmatic quadratic approach (e.g. Cordero et al., 2012; Reddy et al., 2012; Wulfinghoff and Böhlke, 2012; Miehe et al., 2013 Wulfinghoff et al., 2013a,b).

However, the microstructure of a crystal is essentially determined by dislocations. Consequently, no microstructural feature justifies the internal length scale to be fixed. Instead, a more reasonable approach seems to be based on a variable internal length scale as a function of the dislocation state (Groma et al., 2003; Mesarovic et al., 2010).

The quadratic form was recently shown to provide physically unrealistic scaling in the size-dependent response of laminate microstructures under shear (Cordero et al., 2010; Forest and Guéninchault, 2013). Since quadratic forms are unusual in classical dislocation theory, alternative free energy potentials were proposed in the past ten years. Rank-one energies that are linear with respect to the GND densities have been shown to lead to a size-dependent yield stress in certain situations. Additionally motivated by line tension (and more elaborate) arguments, they are used by several authors (Ortiz and Repetto, 1999; Conti and Ortiz, 2005; Ohno and Okumura, 2007; Kametani et al., 2012; Hurtado and Ortiz, 2013).

Asymptotic methods can be used to derive alternative effective potentials for distributions of edge dislocations. The asymptotic derivation of a logarithmic potential by De Luca et al. (2012) accounts for line tension effects at the macroscopic scale. Systematic derivations of backstress distributions were derived in Geers et al. (2013) by means of asymptotic methods.

The choice of a logarithmic energy is inspired by the statistical theory of dislocations of Groma et al. (2003, 2007) and Berdichevsky (2006). Here, the internal length scale of the backstress is determined by the dislocation microstructure (see also Svendsen and Bargmann, 2010; Forest and Guéninchault, 2013). In the latter reference, the rank one and logarithmic formulations were applied to strain gradient plasticity theories involving the full dislocation density tensor instead of the individual GND densities. The constitutive equations were derived and specified in the case of laminate microstructures. However, no analytical or numerical results were provided to solve the laminate problem.

[1] It should be noted that this framework does not fully represent the dislocation-microstructure (like any continuum theory). Additional sources of size effects are not included (e.g. lack of sources, dislocation line curvature effects). Moreover, the application of continuum theories in the micro-regime is often questionable, when the number of dislocations is limited.

The objective of the present work is to investigate the mechanical response of ideal laminate microstructures endowed with strain gradient plasticity properties involving rank one or logarithmic energies. New analytical and numerical solutions are provided in the case of cyclic shear of the periodic laminate. Unusual Bausching effects are predicted that are confronted to experimental evidence from the literature.

The analysis is limited to a laminate material with a single slip system in Section 3, subsequent to the discussion of the general model in Section 2. Analytical and numerical solutions of the laminate shear response are evaluated in order to understand the size-dependence of the overall hardening and yield stress. In addition, the scaling behavior, the form of the dislocation pile-ups and the cyclic loading response are discussed.

The logarithmic energy has irregular properties (non-convexity, non-differentiability). Therefore, a regularized energy is proposed that allows for an interesting physical interpretation. For a long time, it is known that nonconvex potential functions favor the coexistence of different material states or phases in equilibrium. The coexistence ensures minimization of the total potential. Prominent examples in classical thermodynamics and solid mechanics are droplets in vapor, bubbles in a fluid and twinning. For single crystals, it has been shown by Ortiz and Repetto (1999) that the nonconvexity induced by latent hardening with an off-diagonal dominant hardening matrix can imply a non-convexity favoring the development of fine microstructures (see also, Ortiz et al., 2000). The approach by Ortiz and Repetto (1999) is in contrast to the classical plasticity theory based on Drucker's postulate but preferable in the context of micromechanics. Here we prefer, however, working with a convex energy density in order to analyze in a first step the overall composite behavior without additional substructures in the ductile parts of the laminate.

The implicit numerical solution of the rank-one problem is non-trivial, since it is non-smooth and involves sub-differentials. A new regularization technique for the algorithmic treatment of such non-smooth energies is proposed in Section 4. The technique is based on an analogy of the numerical solution of standard plasticity (which is also based on sub-differentials). It is formulated within a potential framework close to the one of Miehe (2011). Moreover, the numerical framework uses features of the micromorphic theory of Forest (2009).

The dislocation density tensor is chosen as additional kinematical quantity. It does not necessitate dislocation density interaction laws, requires less degrees of freedom and is equally defined for all crystal structures. The work is formulated in the small deformation framework. It can be extended to finite deformation in a rather straightforward manner following Aslan et al. (2011).

Notation: A direct tensor notation is preferred throughout the text. Vectors and 2nd-order tensors are denoted by bold letters, e.g. $\boldsymbol{a}$ or $\boldsymbol{A}$. The symmetric part of a 2nd-order tensor $\boldsymbol{A}$ is designated by $\mathrm{sym}(\boldsymbol{A})$. A linear mapping of 2nd-order tensors by a 4th-order tensor is written as $\boldsymbol{A}=\mathbb{C}[\boldsymbol{B}]$. The scalar product and the dyadic product of 2nd-order tensors are denoted, e.g. by $\boldsymbol{A}\cdot\boldsymbol{B}=\mathrm{tr}(\boldsymbol{A}^{\mathrm{T}}\boldsymbol{B})$ and $\boldsymbol{A}\otimes\boldsymbol{B}$, respectively.

2. Two gradient plasticity models

The deformation of a body $\mathcal{B}$ is subsequently described by the displacement field $\boldsymbol{u}$ and the displacement gradient

$$\nabla\boldsymbol{u}=\partial_{x_j}u_i\boldsymbol{e}_i\otimes\boldsymbol{e}_j=\boldsymbol{H}=\boldsymbol{H}^{\mathrm{e}}+\boldsymbol{H}^{\mathrm{p}} \tag{1}$$

with respect to an orthonormal basis $\{\boldsymbol{e}_1,\boldsymbol{e}_2,\boldsymbol{e}_3\}$. Here, $\boldsymbol{H}^{\mathrm{e}}$ and $\boldsymbol{H}^{\mathrm{p}}$ represent the elastic and plastic distorsions, respectively. Analogously, the strain $\boldsymbol{\varepsilon}=\mathrm{sym}(\boldsymbol{H})=\boldsymbol{\varepsilon}^{\mathrm{e}}+\boldsymbol{\varepsilon}^{\mathrm{p}}$ is decomposed.

Additionally, the dislocation density tensor is introduced (Nye, 1953; Kröner, 1958):

$$\boldsymbol{\alpha}=\mathrm{curl}^{\mathrm{T}}(\boldsymbol{H}^{\mathrm{p}})=\epsilon_{ijk}\partial_{x_i}H^p_{lj}\boldsymbol{e}_l\otimes\boldsymbol{e}_k. \tag{2}$$

Here, ϵ_{ijk} denotes the permutation symbol.

The dislocation density tensor determines the net Burgers vector per unit area

$$\boldsymbol{b}=\int_A\boldsymbol{\alpha}\boldsymbol{n}\,\mathrm{d}a, \tag{3}$$

where $\boldsymbol{n}$ represents the outer normal at the infinitesimal area element $\mathrm{d}a$. Besides the Cauchy stress $\boldsymbol{\sigma}$, additional generalized stresses $\boldsymbol{s}$ and $\boldsymbol{M}$ are introduced, which are in general nonsymmetric. These are second-order tensors being work-conjugate to $\dot{\boldsymbol{H}}^{\mathrm{p}}$ and $\dot{\boldsymbol{\alpha}}$, respectively. The virtual power of this internal force system is assumed to be given by

$$\delta\mathcal{P}_{\mathrm{int}}=\int_{\mathcal{B}}\delta p_{\mathrm{int}}\,\mathrm{d}v=\int_{\mathcal{B}}\left(\boldsymbol{\sigma}\cdot\delta\dot{\boldsymbol{\varepsilon}}+\boldsymbol{s}\cdot\delta\dot{\boldsymbol{H}}^{\mathrm{p}}+\boldsymbol{M}\cdot\delta\dot{\boldsymbol{\alpha}}\right)\mathrm{d}v, \tag{4}$$

with $\delta\dot{\boldsymbol{\varepsilon}}=\mathrm{sym}(\nabla\delta\dot{\boldsymbol{u}})$ and $\delta\dot{\boldsymbol{\alpha}}=\mathrm{curl}^{\mathrm{T}}(\delta\dot{\boldsymbol{H}}^{\mathrm{p}})$.

In the absence of volume forces, the virtual power of the external forces is given by

$$\delta\mathcal{P}_{\mathrm{ext}}=\int_{\partial\mathcal{B}_t}\bar{\boldsymbol{t}}\cdot\delta\dot{\boldsymbol{u}}\,\mathrm{d}a+\int_{\partial\mathcal{B}_m}\bar{\boldsymbol{m}}\cdot\delta\dot{\boldsymbol{H}}^{\mathrm{p}}\,\mathrm{d}a, \tag{5}$$

where the integration domains represent Neumann-type boundaries with prescribed tractions $\bar{\boldsymbol{t}}$ and microtractions $\bar{\boldsymbol{m}}$. The

evaluation of the principle of virtual power under static conditions,

$$\delta\mathcal{P}_{\text{int}} = \delta\mathcal{P}_{\text{ext}}, \tag{6}$$

gives, in combination with the chain rule and Gauss' theorem, the field equations at regular points

$$\text{div}\left(\boldsymbol{\sigma}\right) = \mathbf{0}, \quad \boldsymbol{s} + \text{curl}^{\text{T}}(\boldsymbol{M}) = \mathbf{0}. \tag{7}$$

In addition, the principle yields the following Neumann-type boundary conditions on $\partial\mathcal{B}_t$ and $\partial\mathcal{B}_m$

$$\bar{\boldsymbol{t}} = \boldsymbol{\sigma}\boldsymbol{n}, \quad \bar{\boldsymbol{m}} = \boldsymbol{M}\hat{\boldsymbol{n}}, \tag{8}$$

with

$$\hat{\boldsymbol{n}} = -\boldsymbol{\epsilon}\boldsymbol{n} = -(\epsilon_{ijk}\boldsymbol{e}_i \otimes \boldsymbol{e}_j \otimes \boldsymbol{e}_k)(n_l\boldsymbol{e}_l) = -\epsilon_{ijk}n_k\boldsymbol{e}_i \otimes \boldsymbol{e}_j. \tag{9}$$

The power density of the internal forces reads

$$p_{\text{int}} = \boldsymbol{\sigma}\cdot\dot{\boldsymbol{\varepsilon}} + \boldsymbol{s}\cdot\dot{\boldsymbol{H}}^{\text{p}} + \boldsymbol{M}\cdot\dot{\boldsymbol{\alpha}}. \tag{10}$$

Up to this point, the theory is quite general, since it may be applied to single as well as polycrystal plasticity. In the following, the work will focus on single crystal plasticity, where the plastic distorsion is given by the additional kinematical relation

$$\boldsymbol{H}^{\text{p}} = \sum_{\alpha} \gamma_\alpha \boldsymbol{d}_\alpha \otimes \boldsymbol{n}_\alpha, \tag{11}$$

where $\boldsymbol{d}_\alpha$ and $\boldsymbol{n}_\alpha$ denote the slip directions and slip plane normals, respectively. The index α runs over all slip systems.

The equivalent plastic strain is defined by

$$\gamma_{\text{eq}} = \int_0^t \sum_{\alpha} |\dot{\gamma}_\alpha| \, \text{d}\tilde{t}. \tag{12}$$

It is assumed that the volumetric stored energy density has the form

$$W = W_{\text{e}} + W_{\text{g}} + W_{\text{h}}, \tag{13}$$

with $W_{\text{e}} = (\boldsymbol{\varepsilon} - \boldsymbol{\varepsilon}^{\text{p}})\cdot\mathbb{C}[\boldsymbol{\varepsilon} - \boldsymbol{\varepsilon}^{\text{p}}]/2$. The expressions W_{h} and W_{g} are assumed to be functions of $\hat{\nu}$ and $\boldsymbol{\alpha}$, respectively. Here, $\hat{\nu} = (\nu_1, \nu_2, \ldots, \nu_{N_\nu})$ denotes a vector of internal history variables. The functions are assumed normalized, i.e., $W_{\text{h}}(\hat{\mathbf{0}}) = 0$ and $W_{\text{g}}(\mathbf{0}) = \mathbf{0}$. Isotropic hardening is accounted for by W_{h}, while W_{g} models size effects. The evolution of $\hat{\nu}$ is assumed to be given by the rate-independent approach

$$\dot{\nu}_\alpha = \sum_{\beta} f_{\alpha\beta}(\hat{\nu})\,|\dot{\gamma}_\beta| \quad \text{with } f_{\alpha\beta}(\hat{\nu}) \geq 0. \tag{14}$$

The functions $f_{\alpha\beta}$ determine which specific hardening model is applied. For example, if $\hat{\nu} = (\gamma_{\text{eq}})$, it follows that $f_{1\beta} = 1$.

The work at hand investigates the following defect energies-

$$W_{\text{g}}^1 = cGb \parallel \boldsymbol{\alpha} \parallel, \quad W_{\text{g}}^{\ln} = c_0 \parallel \boldsymbol{\alpha} \parallel \ln\frac{\parallel \boldsymbol{\alpha} \parallel}{\alpha_0}, \tag{15}$$

where c is a constant of order unity, G is the macroscopic shear modulus, b is the Burgers vector, α_0 is a constant and c_0 is given by

$$c_0 = \frac{Gb\beta}{2\pi(1-\nu)}, \tag{16}$$

where ν is Poisson's ratio and β is of order unity (in this work $\beta = 1$). The Euclidean norm of the dislocation density tensor is defined as $\parallel \boldsymbol{\alpha} \parallel = \sqrt{\boldsymbol{\alpha}\cdot\boldsymbol{\alpha}}$. More general isotropic approaches of the energy W_{g} may be represented in an irreducible manner in terms of invariants of the dislocation density tensor, as discussed by Boehler (1977).

The rank-one energy W_{g}^1 can be motivated by simple line tension arguments as follows. In many situations, the total elastic energy of a real crystal is well represented by W_{e}. However, the stored elastic energy around dislocations seems to be partially missing in W_{e}, since the regions close to the dislocation cores are not explicitly resolved in the continuum model. In addition, one might assume that the respective energies of a set of statistically stored dislocations (SSDs) may be negligible, since SSDs tend to form di- and multipoles. This implies a mutual screening of the individual stress fields and lower energies. Finally, it may be assumed that all other dislocation interactions are accounted for in W_{e}. Then, the remaining energy that needs to be accounted for is the stored elastic energy around geometrically necessary dislocations. The associated energy density is proportional to the amount of GNDs, since the interactions are assumed to be already represented by W_{e}. This explains the form of W_{g}^1 in Eq. (15). For additional arguments see Ortiz and Repetto (1999) and Hurtado and Ortiz (2012, 2013).

The logarithmic energy $W_{\mathrm{g}}^{\ln}$ (Eq. (15)) is motivated by the form of the associated backstress (Forest and Guéninchault, 2013). It turns out that the approach $W_{\mathrm{g}}^{\ln}$ leads to a backstress which is formally close to the one derived in the statistical theory of Groma et al. (2003),[2] given by

$$-\frac{Gc_1}{2\pi(1-\upsilon)\rho}\partial_{x_1}^2\gamma \tag{17}$$

for a single slip situation with slip direction $\boldsymbol{e}_1$. Here, ρ denotes the total dislocation density. In the two-dimensional single slip regime, the backstress involves the Laplacian of the plastic slip, as postulated by Aifantis (1987). However, the internal length scale is not interpreted as a material constant but determined by the dislocation microstructure, if $W_{\mathrm{g}}^{\ln}$ is applied. This point is discussed in detail in Section 3.2.1.

The subsequent sections investigate the features of the rank-one and logarithmic energies W_{g}^{1} and $W_{\mathrm{g}}^{\ln}$, respectively. Since the logarithmic energy is neither smooth nor convex, a regularization will also be discussed.

The stresses $\boldsymbol{\sigma}$ and $\boldsymbol{M}$ are assumed to be energetic, i.e.

$$\boldsymbol{\sigma}=\partial_{\boldsymbol{\varepsilon}}W,\quad \boldsymbol{M}=\partial_{\boldsymbol{\alpha}}W. \tag{18}$$

The dissipation inequality can be shown to be given by

$$\mathcal{D}=p_{\mathrm{int}}-\dot{W}=\sum_{\alpha}\left(\tau_{\alpha}^{\mathrm{eff}}-q_{\alpha}\,\mathrm{sgn}\left(\dot{\gamma}_{\alpha}\right)\right)\dot{\gamma}_{\alpha}\geq 0 \tag{19}$$

with $\tau_{\alpha}^{\mathrm{eff}}=(\boldsymbol{\sigma}+\boldsymbol{s})\cdot(\boldsymbol{d}_{\alpha}\otimes\boldsymbol{n}_{\alpha})$ and $q_{\alpha}=\sum_{\beta}f_{\alpha\beta}\partial_{\nu_{\beta}}W_{\mathrm{h}}$. A possible flow rule, satisfying the dissipation inequality (19), is given by the following power law:

$$\dot{\gamma}_{\alpha}=\mathrm{sgn}\left(\tau_{\alpha}^{\mathrm{eff}}\right)\dot{\gamma}_0\left\langle\frac{|\tau_{\alpha}^{\mathrm{eff}}|-(\tau^{\mathrm{C}}+q_{\alpha})}{\tau^{\mathrm{D}}}\right\rangle^{p}. \tag{20}$$

Here, τ^{C} is the initial yield stress, $\dot{\gamma}_0$ is a reference shear rate, p is the strain rate sensitivity and τ^{D} is a drag stress.

If the stored energy is not differentiable at $\boldsymbol{\alpha}=\boldsymbol{0}$, the symbol ∂ in Eq. $(18)_2$ is interpreted as a sub-differential operator (see, e.g., Han and Reddy, 2013), i.e.

$$\boldsymbol{M}|_{\boldsymbol{\alpha}=\boldsymbol{0}}\in\{\boldsymbol{M}\colon W_{\mathrm{g}}(\boldsymbol{\alpha})-\boldsymbol{M}\cdot\boldsymbol{\alpha}\geq 0\ \ \forall\ \ \boldsymbol{\alpha}\}. \tag{21}$$

This can be interpreted as follows. If the stress $\boldsymbol{M}$ is applied at a material point, $\boldsymbol{\alpha}$ will take a value which minimizes the expression $W_{\mathrm{g}}(\boldsymbol{\alpha})-\boldsymbol{M}\cdot\boldsymbol{\alpha}$. For small values of $\boldsymbol{M}$, the minimum is given by $\boldsymbol{\alpha}=\boldsymbol{0}$. However, for sufficiently large values of $\boldsymbol{M}$, the value of $\boldsymbol{\alpha}$ can be determined from the stationarity condition $\boldsymbol{M}=\partial_{\boldsymbol{\alpha}}W_{\mathrm{g}}$.

Example. If W_{g} is given by $W_{\mathrm{g}}^{1}=cGb\parallel\boldsymbol{\alpha}\parallel$, it follows that $\boldsymbol{\alpha}=\boldsymbol{0}$ if

$$\boldsymbol{M}\cdot\tilde{\boldsymbol{\alpha}}\leq W_{\mathrm{g}}^{1}(\tilde{\boldsymbol{\alpha}})=cGb\parallel\tilde{\boldsymbol{\alpha}}\parallel\quad\forall\,\tilde{\boldsymbol{\alpha}} \tag{22}$$

$$\Leftrightarrow\boldsymbol{M}\cdot\tilde{\boldsymbol{\alpha}}\leq\parallel\boldsymbol{M}\parallel\parallel\tilde{\boldsymbol{\alpha}}\parallel\leq cGb\parallel\tilde{\boldsymbol{\alpha}}\parallel\quad\forall\,\tilde{\boldsymbol{\alpha}}. \tag{23}$$

Hence, it is found that

$$\begin{cases}\boldsymbol{M}\in\{\boldsymbol{M}\colon\varphi(\boldsymbol{M})\leq 0\}, & \text{if } \boldsymbol{\alpha}=\boldsymbol{0}\\ \boldsymbol{M}=cGb\dfrac{\boldsymbol{\alpha}}{\parallel\boldsymbol{\alpha}\parallel}, & \text{else.}\end{cases} \tag{24}$$

with $\varphi(\boldsymbol{M})=\parallel\boldsymbol{M}\parallel-cGb$.

Remark. Note that the generalized stress $\boldsymbol{M}$ can be computed uniquely from $\boldsymbol{\alpha}$ only if $\boldsymbol{\alpha}\neq\boldsymbol{0}$. This makes analytical solutions as well as the numerical implementation difficult. The same problem arises in rate-independent rigid plasticity, where the stress can only be computed from the plastic slip rate if this is non-vanishing. Possible regularization techniques include the introduction of small elastic strains or the approximation of the rate-independent model by, e.g., a power law with a large rate-sensitivity. The introduction of elastic strains usually implies better convergence properties. Therefore, the work at hand introduces an analogue regularization technique which will be discussed later.

Possible other numerical strategies concerning this problem are discussed in Kametani et al. (2012) as well as Hurtado and Ortiz (2013).

[2] Since Groma's work represents a two-dimensional single slip theory, this comparison is made for that situation.

3. Shearing of a periodic laminate

In this section, the theory introduced in Section 2 is applied to an elasto-plastic laminate microstructure exposed to plane strain (Fig. 1). Similar problems have been investigated by Cordero et al. (2010), Aslan et al. (2011) as well as Forest and Guéninchault (2013). The laminate consists of periodic elastic (hard) and elasto-plastic (soft) layers. The widths of the hard and soft layers are given by h and s, respectively. It is assumed that the plastic layer deforms in single slip with horizontal slip direction $\boldsymbol{d} = \boldsymbol{e}_1$ and vertical slip plane normal $\boldsymbol{n} = \boldsymbol{e}_2$, i.e. $\boldsymbol{H}^{\mathrm{p}} = \gamma \boldsymbol{e}_1 \otimes \boldsymbol{e}_2$. Per definition, the plastic shear strain in the hard phase is set to zero, $\gamma = 0$.

The dislocation density tensor (2) can be expressed in terms of the edge density $\rho_{\perp} = -\partial_{x1}\gamma$

$$\boldsymbol{\alpha} = -\rho_{\perp}\boldsymbol{e}_1 \otimes \boldsymbol{e}_3. \tag{25}$$

The quantity $\rho_{\perp}$ represents the total Burgers vector amount per unit area of edge dislocations. Note that its unit ($\mu\mathrm{m}^{-1}$) differs from the unit of the total line length per unit volume ρ, given by $\mu\mathrm{m}^{-2}$.

Subsequently, the unit cell in Fig. 1 (right) is considered. The origin of the coordinate system is located in the center of the soft phase.

The shear deformation is assumed to be given by the following displacement field:

$$\boldsymbol{u} = \bar{\gamma} x_2 \boldsymbol{e}_1 + \tilde{u}(x_1)\boldsymbol{e}_2. \tag{26}$$

The deformation is driven by the macroscopic shear strain $\bar{\gamma}$ (not to be confused with the average of γ).[3]

Since $\tilde{u}(x_1)$ is a periodic fluctuation, the following relations have to be satisfied:

$$\int_{-s/2}^{s/2+h} \tilde{u}\, \mathrm{d}x_1 = 0, \quad \int_{-s/2}^{s/2+h} \tilde{u}'\, \mathrm{d}x_1 = 0. \tag{27}$$

Henceforth, $(\bullet)'$ denotes the derivative with respect to x_1. From Eq. (26) and the definition of $\boldsymbol{H}^{\mathrm{p}}$, the displacement gradient and elastic strain are found to be

$$\boldsymbol{H} = \bar{\gamma}\boldsymbol{e}_1 \otimes \boldsymbol{e}_2 + \tilde{u}'(x_1)\boldsymbol{e}_2 \otimes \boldsymbol{e}_1 \tag{28}$$

and

$$\boldsymbol{\varepsilon}^{\mathrm{e}} = (\bar{\gamma} + \tilde{u}' - \gamma)\mathrm{sym}(\boldsymbol{e}_1 \otimes \boldsymbol{e}_2), \tag{29}$$

respectively. The material is taken to be elastically isotropic and homogeneous, for the sake of simplicity. Therefore, Eq. (29) implies that all stress components vanish, except for $\sigma_{12} = \sigma_{21}$. From the linear momentum balance $\sigma_{12}{}'(x_1) = 0$ (see Eq. $(7)_1$), it follows that the stress and the elastic strain are homogeneous

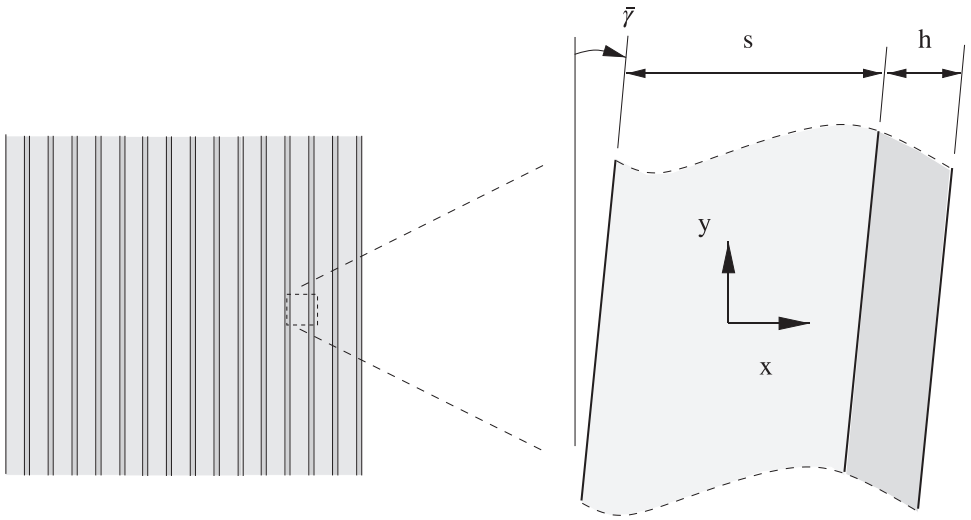

Fig. 1. Undeformed laminate material and deformed unit cell. The dark elastic phase is hard (h) and the light elasto-plastic phase is soft (s).

[3] Assuming isotropic elastic properties, it can be shown that the fluctuation in $\boldsymbol{e}_1$-direction vanishes using the linear momentum balance $(7)_1$.

$$\varepsilon_{12}^{\mathrm{e}} = \frac{1}{2}(\bar{\gamma} + \tilde{u}' - \gamma) = \frac{\sigma_{12}}{2G} = \text{const.} \tag{30}$$

Assuming the defect energy W_{g} to be a function of $\| \boldsymbol{\alpha} \|$, the generalized stress $\boldsymbol{M}$ reads

$$\boldsymbol{M} = \partial_{\boldsymbol{\alpha}} W_{\mathrm{g}} = \partial_{\| \boldsymbol{\alpha} \|} W_{\mathrm{g}} \frac{\boldsymbol{\alpha}}{\| \boldsymbol{\alpha} \|} = - \ \mathrm{sgn}\,(\rho_{\vdash}) \partial_{|\rho_{\vdash}|} W_{\mathrm{g}} \boldsymbol{e}_1 \otimes \boldsymbol{e}_3 = M(x_1) \boldsymbol{e}_1 \otimes \boldsymbol{e}_3. \tag{31}$$

All other components of $\boldsymbol{M}$ are assumed to vanish.[4] From the balance equation $(7)_2$, it follows that

$$s_{12} - M' = 0. \tag{32}$$

Throughout this section, the isotropic hardening contribution will be neglected, i.e. $W_{\mathrm{h}} = 0$.

3.1. Rank-one defect energy

3.1.1. Analytical solution

For the laminate, the following energy is adopted:

$$W_{\mathrm{g}}^1 = cGb \ \| \boldsymbol{\alpha} \| = cGb \, |\rho_{\vdash}|, \tag{33}$$

where c is of order unity (Ortiz and Repetto, 1999). According to Eq. (31), the generalized stress M reads

$$M = - \frac{\rho_{\vdash}}{|\rho_{\vdash}|} cGb = - \ \mathrm{sgn}\,(\rho_{\vdash}) cGb \quad \text{if } |\rho_{\vdash}| > 0$$

$$|M| \leq cGb \quad \text{if } |\rho_{\vdash}| = 0. \tag{34}$$

where the second line follows from Eq. (24).

Subsequently, a monotonous shear deformation in the positive direction is prescribed such that the following relations hold in the soft phase:

$$\tau^{\mathrm{eff}} \geq \tau^{\mathrm{C}}, \quad \dot{\gamma} \geq 0. \tag{35}$$

In a first step of the analysis, the flow rule (20) is assumed to be given by a linear visco-plastic relation, i.e.

$$\dot{\gamma} = \dot{\gamma}_0 \frac{\tau^{\mathrm{eff}} - \tau^{\mathrm{C}}}{\tau^{\mathrm{D}}} \Leftrightarrow \tau^{\mathrm{eff}} = \tau^{\mathrm{C}} + \tau^{\mathrm{D}} \frac{\dot{\gamma}}{\dot{\gamma}_0}. \tag{36}$$

Note that the analysis is finally aiming at a rate-independent formulation. At the present stage, the viscous term is still kept to prove that the model leads to a size effect in the model response. Afterwards, viscous terms will be neglected. With Eq. (36), the dissipation (19) reads

$$\mathcal{D} = \tau^{\mathrm{eff}} \dot{\gamma} = \tau^{\mathrm{C}} \dot{\gamma} + \tau^{\mathrm{D}} \frac{\dot{\gamma}^2}{\dot{\gamma}_0}. \tag{37}$$

A symmetric slip profile is expected with

$$\gamma'(x_1) \geq 0 \quad \forall \, x_1 \in (-s/2, 0), \quad \gamma'(x_1) \leq 0 \quad \forall \, x_1 \in (0, s/2). \tag{38}$$

A cuboid-shaped volume $\Delta\mathcal{B}$ is considered, as illustrated in Fig. 2. For this volume, the equality of external and internal powers is evaluated in the following.

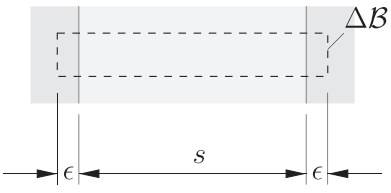

Fig. 2. Illustration of the integration volume $\Delta\mathcal{B}$.

[4] Note that this is a quite strong assumption, if $\boldsymbol{\alpha} = \boldsymbol{0}$ and a non-smooth energy are considered. For $\boldsymbol{\alpha} \neq \boldsymbol{0}$, this is a mere consequence of the constitutive equation for $\boldsymbol{M}$.

The power of the external forces reads

$$\mathcal{P}_{\text{ext}}(\Delta\mathcal{B}) = \int_{\partial(\Delta\mathcal{B})} \boldsymbol{t}\cdot\dot{\boldsymbol{u}}\,\mathrm{d}a + \int_{\partial(\Delta\mathcal{B})} \boldsymbol{m}\cdot\dot{\boldsymbol{H}}^{\mathrm{p}}\,\mathrm{d}a. \tag{39}$$

The second integral vanishes, as shown in Appendix A.

From Gauss' theorem as well as the linear momentum balance $\operatorname{div}(\boldsymbol{\sigma}) = \boldsymbol{0}$ and the boundary condition $\boldsymbol{t} = \boldsymbol{\sigma}\boldsymbol{n}$ (Eqs. $(7)_1$ and $(8)_1$), it follows that

$$\mathcal{P}_{\text{ext}}(\Delta\mathcal{B}) = \int_{\partial(\Delta\mathcal{B})} \boldsymbol{t}\cdot\dot{\boldsymbol{u}}\,\mathrm{d}a = \int_{\Delta\mathcal{B}} \boldsymbol{\sigma}\cdot\dot{\boldsymbol{\varepsilon}}\,\mathrm{d}v. \tag{40}$$

On the contrary, the power of internal forces is given by

$$\mathcal{P}_{\text{int}}(\Delta\mathcal{B}) = \int_{\Delta\mathcal{B}} p_{\text{int}}\,\mathrm{d}v \overset{(19)}{=} \int_{\Delta\mathcal{B}} (\dot{W} + \mathcal{D})\,\mathrm{d}v. \tag{41}$$

Finally, the equality $\mathcal{P}_{\text{ext}}(\Delta\mathcal{B}) = \mathcal{P}_{\text{int}}(\Delta\mathcal{B})$ can be represented as follows (after some rearrangements, see Eq. (36) and Appendix B):

$$2cGb\,\dot{\gamma}(0) + (\tau^{\mathrm{C}} - \sigma_{12}) \int_{-s/2-\epsilon}^{s/2+\epsilon} \dot{\gamma}\,\mathrm{d}x_1 + \frac{\tau^{\mathrm{D}}}{\dot{\gamma}_0} \int_{-s/2-\epsilon}^{s/2+\epsilon} \dot{\gamma}^2\,\mathrm{d}x_1 = 0. \tag{42}$$

This relation allows to show that there is a size effect on the overall strength of the laminate. In order to prove this, assume that there was no size effect. Then, the solution would be the classical one with $\dot{\gamma} = \text{const.}$ in the soft phase. In this case, Eq. (42) would reduce to

$$\sigma_{12} = \tau^{\mathrm{C}} + \tau^{\mathrm{D}}\frac{\dot{\gamma}}{\dot{\gamma}_0} + \frac{2cGb}{s}, \tag{43}$$

after division by $\dot{\gamma}$'s. Since the last term scales like $1/s$, the assumption that there is no size effect must be wrong.

The rate-independent limit can be considered by setting $\dot{\gamma}_0 \to \infty$. In this case, the last integral in Eq. (42) vanishes. As before, a fully plastic situation is considered, i.e., the yield condition $\tau^{\text{eff}} = \sigma_{12} + s_{12} = \tau^{\mathrm{C}}$ is assumed to hold everywhere in the soft phase. Then,

$$M' \overset{(32)}{=} s_{12} = -(\sigma_{12} - \tau^{\mathrm{C}}) = \text{const.} \tag{44}$$

$$\Rightarrow M = -(\sigma_{12} - \tau^{\mathrm{C}})x_1, \tag{45}$$

where the constant of integration vanishes due to the symmetry requirement $|M(-s/2)| = |M(s/2)|$. Since $|M(x_1)|$ is not constant, the dislocation density $\rho_{\vdash} = -\gamma'$ must vanish (comp. Eq. (34)). Therefore, $\gamma = \text{const.}$ and from Eq. (42) it follows that

$$\sigma_{12} = \tau^{\mathrm{C}} + \frac{2cGb}{s}. \tag{46}$$

This equation holds in the plastic regime. Clearly, the application of the rank-one energy increases the macroscopic yield stress by $2cGb/s$, i.e., the increase scales inversely with the size of the soft phase (see Fig. 3). The same scaling behavior has been found by Ohno and Okumura (2007) for a spherical grain, also using a rank-one energy. The authors concentrated on the overall mechanical response without having to compute the fields inside of the grains. As illustrated in Fig. 3, the dislocations localize in dislocation walls at the elasto-plastic interface.

In the plastic regime, the plastic shear strain follows from Eqs. (30) and (46) and the constraint $(27)_2$

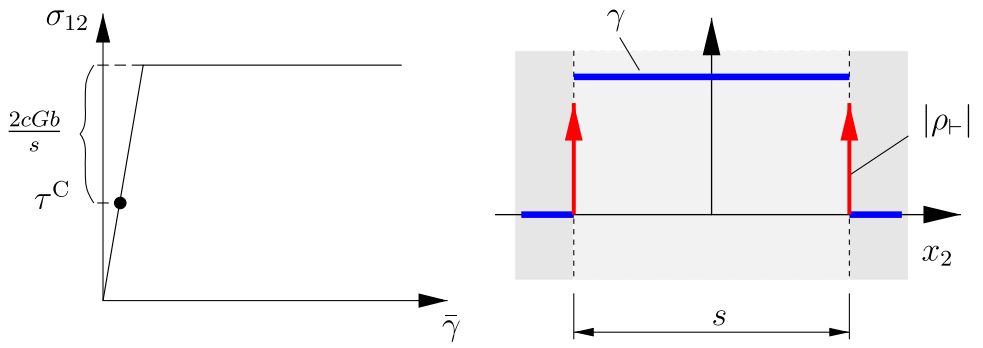

Fig. 3. Macroscopic shear stress strain curve for the rank-one energy. The increase of the overall yield point scales inversely with the size of the soft phase.

$$\gamma = \frac{s+h}{s}\left(\bar{\gamma} - \frac{\tau^{\mathrm{C}} + 2cGb/s}{G}\right). \tag{47}$$

In addition to these results, the system behavior can be characterized as follows:

- For the material parameters of aluminum ($G = 26.12$ GPa and $b = 0.286$ nm) and $c = 1$, the size effect becomes important when the system size is below ~ 10 μm.
- The plastic shear strain is constant in the bulk, i.e., the dislocations form singularities (walls) at the boundaries.
- The backstress is constant (w.r.t. space) in the bulk. During the first period, it increases and thereby impedes any plastic deformation. Therefore, the overall deformation is purely elastic during this period. At a certain point, the plastic deformation starts and the backstress remains constant afterwards. Its value is given by $2cGb/s$.

3.2. Logarithmic energy

3.2.1. Motivation

This section investigates the following defect energy:

$$W_{\mathrm{g}}^{\ln} = c_0 \,\|\boldsymbol{\alpha}\|\, \ln\frac{\|\boldsymbol{\alpha}\|}{\alpha_0}, \tag{48}$$

with the constant c_0 as defined in Eq. (16). The energy is motivated by the statistical theory of dislocations by Groma et al. (2003). The authors derive a backstress term which involves the second gradient of slip as postulated by Aifantis (1987). However, their theory involves an internal length scale which is given by $1/\sqrt{\rho}$, where ρ denotes the total dislocation density.

In pure metals, the geometrical characteristics of the microstructure are essentially determined by the dislocation arrangement. This is a strong argument for a (variable) internal length scale, which is determined by the available dislocation field variables (instead of a constant length scale parameter, see also Forest and Sedláček, 2003 where this dependency is derived from a dislocation line tension model).

It is demonstrated subsequently that the approach (48) leads to a backstress which is similar to that of Groma et al. (2003). However, it should be mentioned that this energy is neither convex nor smooth with respect to the dislocation density tensor (a regularization will be discussed at a later stage).

For the laminate problem, the generalized stress M reads (see Eq. (31))

$$M = -\,\operatorname{sgn}(\rho_{\vdash})\, c_0\left(\ln\frac{|\rho_{\vdash}|}{\alpha_0} + 1\right). \tag{49}$$

In this section, rate-independent plasticity will be considered based on the yield criterion

$$f = |\tau^{\mathrm{eff}}| - \tau^{\mathrm{C}} \leq 0. \tag{50}$$

Here, the effective stress reads

$$\tau^{\mathrm{eff}} = (\boldsymbol{\sigma} + \boldsymbol{s})\cdot(\boldsymbol{d} \otimes \boldsymbol{n}) = \sigma_{12} + s_{12} \overset{(32)}{=} \sigma_{12} + M'. \tag{51}$$

With Eq. (49) and $M' = (\partial_{\rho_{\vdash}} M)(\partial_{x_1}\rho_{\vdash})$, it follows that

$$\tau^{\mathrm{eff}} = \tau - \frac{c_0}{|\rho_{\vdash}|}\partial_{x_1}\rho_{\vdash} = \tau + \frac{G\beta}{2\pi(1-\nu)}\frac{b}{|\rho_{\vdash}|}\partial_{x_1}^2\gamma. \tag{52}$$

Here, the second term can be interpreted as a backstress. Note that the backstress involves no internal length scale parameter. Instead, the internal length scale, $\sqrt{b/\rho_{\vdash}}$, is determined by the dislocation microstructure. In contrast to the backstress of Groma et al. (2003), the internal length scale is determined by the GND-density $\rho_{\vdash}$ instead of the total density ρ. Hence, the influence of statistically stored dislocations (SSDs) is ignored. This question will be addressed at a later point. For the moment, GND-dominated problems will be focused on. Therefore, a homogeneous initial GND-density $|\rho_{\vdash}| = \alpha_0$ will be assumed to be given. In addition, it is assumed that the SSD-density is equal to or less than α_0.

3.2.2. Analytical solution

The soft phase is assumed to be under plastic loading, with $\tau^{\mathrm{eff}} = \tau^{\mathrm{C}}$ in the soft phase. In this case,

$$M' \overset{(32)}{=} s_{12} = -(\sigma_{12} - \tau^{\mathrm{C}}) = \text{const.} \tag{53}$$

$$\Rightarrow M = -(\sigma_{12} - \tau^{\mathrm{C}})x_1, \tag{54}$$

where, again, the constant of integration vanishes due to the symmetry requirement $|M(-s/2)| = |M(s/2)|$. The plastic slip γ can be derived from the equality of Eqs. (49) and (54), which yields a differential equation for γ. The solution reads

$$\gamma = \frac{\alpha_0 L}{e}\left(\exp\left(\frac{s}{2L}\right) - \exp\left(-a\frac{x_1}{L}\right)\right) \quad \text{with } L = \frac{c_0}{\sigma_{12} - \tau^c}, \tag{55}$$

where the matching conditions $\gamma(-s/2) = \gamma(s/2) = 0$ have been exploited and where $e = \exp(1)$. The variable a is defined by $a = \operatorname{sgn}(\gamma')$ and is assumed positive in $(-s/2, 0)$ and negative in $(0, s/2)$.[5]

From Eqs. $(27)_2$ and (30) the macroscopic stress strain relation follows:

$$\bar{\gamma} = \frac{\alpha_0 L}{e(s+h)}\left(\exp\left(\frac{s}{2L}\right)(s-2L) + 2L\right) + \frac{\sigma_{12}}{G}. \tag{56}$$

The solution is evaluated for the following material parameters.

E (GPa)	ν	τ^c (MPa)	b (nm)	β	α_0/b [(μm^{-2})]
70	0.34	10	0.286	1	1

Here, E and ν denote Young's modulus and Poisson's ratio. A very thin hard phase with negligible width h is considered ($h/s = 10^{-6}$ for the analytical solution).

The macroscopic stress–strain curve (56) is illustrated in Fig. 4. A clear size effect is visible. Apparently, mainly the overall

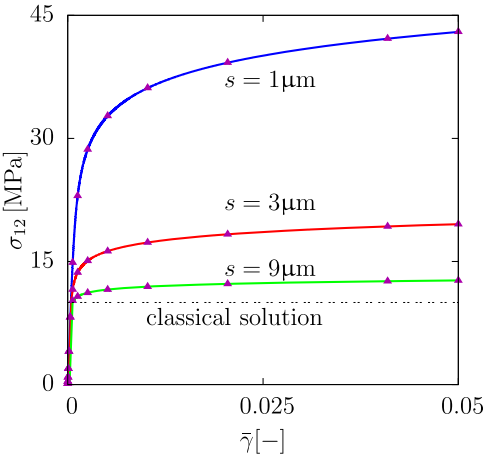

Fig. 4. Macroscopic stress–strain diagram for three different sizes. Analytical (lines) and regularized, numerical (triangles) solution for the logarithmic potential.

yield stress is affected. The hardening shows less size dependence. It is remarkable that the model provides a size-dependent yield stress and non-linear kinematic hardening.

The microscopic plastic shear strain γ and dislocation density are shown in Fig. 5. Dislocation pile-ups are observed at the boundaries of the soft phase.

Since there is no distinct yield stress, the evaluation of the scaling behavior is based on the offset yield stress at 0.2% plastic strain. Fig. 6 shows the offset yield stress as a function of the inverse of the size $1/s$. For comparison, the results obtained from the rank-one energy are illustrated, in addition. For $c = 1.2$, the scaling behavior of both energies is similar in the considered range.

3.2.3. *Regularization of the logarithmic energy*

The length scale $\sqrt{b/\rho_+}$ of the backstress in Eq. (52) is determined by the GNDs. This was the main motivation of the logarithmic energy (Eq. (48)). In the following, the theory is extended to problems which are not fully GND-dominated. For that purpose, the following regularization is introduced (see Fig. 7).

[5] It is noteworthy that the solution depends on α_0, although this constant does neither appear in the field equation $\tau^c = \sigma_{12} + c_0\partial^2_{x1}\gamma/|\partial_{x1}\gamma|$ nor in the matching condition $\gamma(\pm s/2) = 0$.

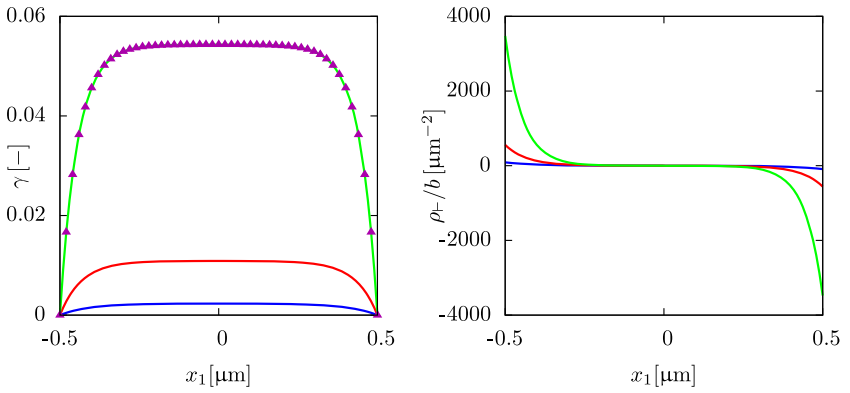

Fig. 5. Plastic slip γ and dislocation density $\rho_{\vdash}/b$ for the smallest size ($s = 1\ \mu$m), according to the logarithmic model. Left: plastic slip at 0.3, 1.1 and 5% macroscopic strain (triangles: regularized, numerical solution). Right: corresponding GND-densities.

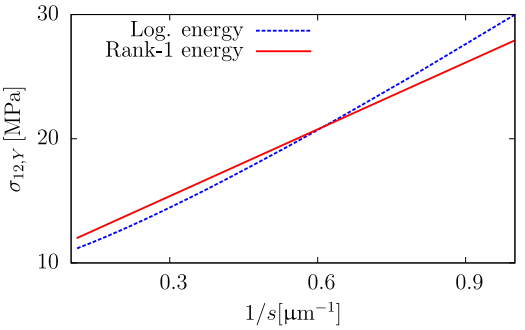

Fig. 6. Scaling-comparison of the two energies for $c = 1.2$. The shear stress values of the logarithmic energy correspond to 0.2% plastic shear strain.

$$W_g = \begin{cases} \frac{1}{2}\frac{c_0}{b} l^2 \,\|\boldsymbol{\alpha}\|^2, & \|\boldsymbol{\alpha}\| < \alpha_L \\ c_0 \,\|\boldsymbol{\alpha}\| \,\ln\frac{\|\boldsymbol{\alpha}\|}{\alpha_0} + W_0 & \text{else.} \end{cases} \tag{57}$$

In the region of small GND-densities, the energy is replaced by a quadratic potential. The internal length scale l, the transition density α_L and the offset energy W_0 are chosen such that W_g, $\partial_{\|\boldsymbol{\alpha}\|} W_g$ and $\partial^2_{\|\boldsymbol{\alpha}\|} W_g$ are continuous at the transition point $\|\boldsymbol{\alpha}\| = \alpha_L$. As a result

$$\alpha_L = \alpha_0, \quad l^2 = \frac{b}{\alpha_0}, \quad W_0 = \frac{c_0 \alpha_0}{2}. \tag{58}$$

The regularized energy (57) is convex, normalized and twice differentiable. The backstress for the laminate problem reads

$$x = \begin{cases} -\frac{c_0}{\alpha_0}\partial^2_{x_1}\gamma, & |\rho_{\vdash}| < \alpha_0, \\ -\frac{c_0}{|\rho_{\vdash}|}\partial^2_{x_1}\gamma & \text{else.} \end{cases} \tag{59}$$

The solution based on the regularized model has been obtained numerically by finite elements. Figs. 4 and 5 compare the analytical and numerical solution. It should be noted that for $\alpha_0 \to \infty$ a quadratic energy is recovered, as has been used by

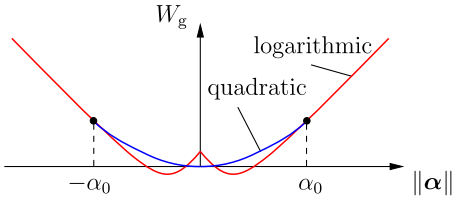

Fig. 7. Regularization of the logarithmic energy.

numerous authors. For this case, the solution for the laminate problem has been investigated by Forest and Guéninchault (2013). In contrast to Fig. 4 the overall stress–strain response is characterized by a linear kinematic hardening response (see Forest and Guéninchault, 2013, Fig. 3).

3.2.4. Interpretation of the regularization

If the dislocation microstructure is GND-dominated, the internal length scale of the laminate model is supposed to be $\sqrt{b/\rho_{\vdash}}$, i.e., determined by the GND-density. Therefore, the threshold α_0 in Eq. (59) should be chosen such that it clearly indicates whether the microstructure at a given point is GND- or SSD-dominated. If the SSD-density is nearly homogeneous, a reasonable choice of α_0 is the SSD-density itself. If the SSD-density is not constant, α_0 might be interpreted as a characteristic SSD-density. In this case, the logarithmic energy is applied, if $|\rho_{\vdash}| > \alpha_0$, i.e., if the problem is GND-dominated.

However, the quadratic energy is applied if $|\rho_{\vdash}| < \alpha_0$, i.e., when the SSDs dominate. As an interesting feature, the internal length scale $\sqrt{b/\alpha_0}$ of the backstress (59) is then determined by the SSD-density.

In both cases, the backstress (59) is approximately given by

$$x \approx -\frac{c_0/b}{\rho}\partial^2_{x_1}\gamma. \tag{60}$$

This backstress coincides with Groma's representation. In this sense, the energy approach (57) reduces to a gradient plasticity approximation of Groma's theory. Eq. (60) is valid except the case $\rho_{\mathrm{SSD}} \approx \rho_{\mathrm{GND}}$. In this case, the backstress is overestimated by a factor of two.

Fig. 8 shows the influence of the parameter α_0 on the size effect. The parameter α_0 has been varied within three orders of magnitude ($\alpha_0/b = 0.1, 1$ and $10\ \mu\mathrm{m}^{-2}$). Obviously, a variation of α_0 within orders of magnitude is indeed necessary in order

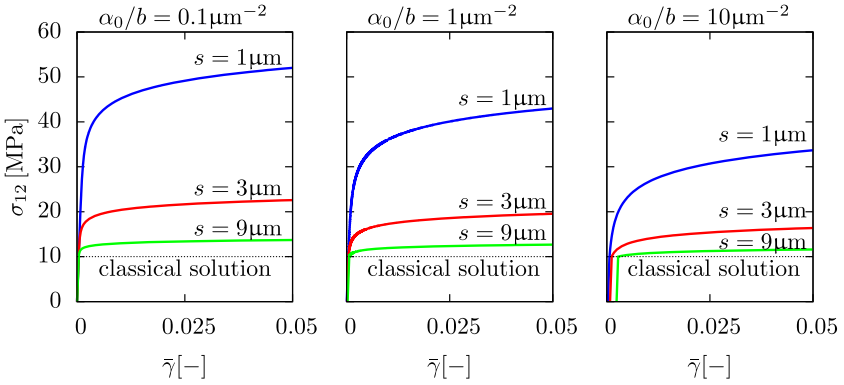

Fig. 8. Influence of α_0 on the overall size effect, according to the regularized logarithmic model.

to significantly influence the results. Hence, the model sensitivity with respect to changes of α_0 is smaller than might have been expected.

One might hope that a rough estimate of the SSD-density could be sufficient to achieve a reasonable guess of the parameter α_0. In particular, the overestimation of the backstress in the case $\rho_{\mathrm{GND}} = \rho_{\mathrm{SSD}}$ by a factor of two has less consequences than expected, since a multiplication of α_0 by two has a minor influence on the results.

Here, the sensitivity of σ_{12} with respect to changes of α_0 has been investigated for a specific set of material parameters. A more general sensitivity analysis, as given in Appendix C, leads to similar results.

3.3. Cyclic behavior of the laminate

The laminate is now submitted to one full cycle $\bar{\gamma} = \pm 0.05$. The hysteresis loops σ_{12} vs. $\bar{\gamma}$ for both rank one and logarithmic potentials are represented in Fig. 9 for $s = 3\ \mu\mathrm{m}$. In the absence of isotropic hardening, the loops are stabilized after one full cycle. They are characterized by pure kinematic hardening. The influence of the backstress is clearly observable. The curves in Fig. 9 have been obtained numerically. Therefore, both models are regularized as explained in the previous sections. One striking feature of the results is that the obtained loops have inflection points. According to the rank one model the first unloading stage is characterized by reverse plasticity at a constant negative shear stress. When $\bar{\gamma}$ goes through zero again, the overall shear stress experiences a jump of the same magnitude as computed analytically for monotonic loading in Sections 3.1 and 3.2. The loop with inflections obtained for the logarithmic potential is similar but smoother and displays smooth nonlinear kinematic hardening. A similar hysteresis loop was obtained by Ohno and Okumura (2008) for the rank one model.

The type of non-linear kinematic hardening observed for both models corresponds to Asaro's type KIII model, corresponding to a *first in/last out* sequence of dislocation motion (Asaro, 1975). It is considered by Asaro as the most perfect form

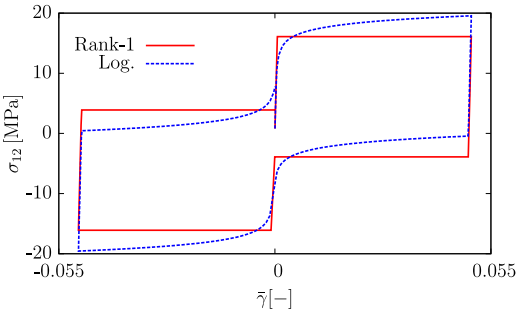

Fig. 9. Cyclic loading for $s=3$ μm.

of recovery of plastic memory. Such stress–strain loops display inflection points that are observed in some materials, see Asaro (1975) for a Nimonic alloy, but such observations have also been made in several Nickel based superalloys. It is usually attributed to substructural recovery on the microscale, for instance pile-up formation and destruction at γ' precipitates. In the present simple single crystal model, it is the single active hardening mechanism induced by strain gradient plasticity and the presence of the hard phase in the laminate. It represents an accurate continuum description of dislocation piling-up and unpiling-up phenomena.

The experimental evidence of such loops with inflections is illustrated in Figs. 10 and 11 in the case of polycrystalline Fe–Cr and Al–Cu–Mg alloys, respectively. The first loop in Fig. 10 (left) exhibits two inflection points which vanish after a few

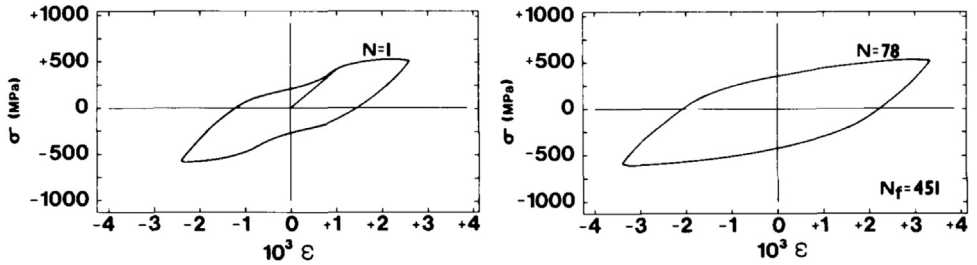

Fig. 10. Shape of the stress–strain hysteresis loop as a function of the number N of cycles for a Fe–19 wt% Cr alloy aged at 923 K for 72 h and mechanically tested at room temperature: $N=1$ (left), $N=48$ (right, N_f indicates the number of cycles to failure), after Taillard and Pineau (1982).

cycles and the usual shape with still a strong Bauschinger effect is retrieved in Fig. 10 (right). Fig. 11 shows that the amount of plastic reversibility is controlled by the annealing degree of the dislocation microstructure. Further evidence of loops with inflections in the cyclic behavior of FCC alloys can be found in the recent contribution by Proudhon et al. (2008) dealing with aluminium alloys. The common characteristics of these FCC alloys are that they all contain a population of nonshearable intragranular precipitates. This distribution of particles represents the first series of obstacles to be overcome by dislocations for the plasticity to start. The distance between precipitates presents a small scatter and the average value is the characteristic length responsible for the size-dependent yield limit. This distance is comparable to the width s in our ideal laminate model. As illustrated by the TEM observations by Stoltz and Pelloux (1974, 1976), Taillard and Pineau (1982) and Proudhon et al. (2008), dislocation loops multiply around precipitates and can be destroyed after reverse loading unless the material is annealed before reversing the load, see Fig. 11, or unless the multiplication of forest dislocations or cross-slip effects limit the reversibility of cyclic plasticity. The simulations based on the logarithmic potential provide smooth loops that are closer to the experimental shapes. The present authors have not found experimental evidence of such effects in single crystals in the literature. This is probably due to the fact that the effect is observed in alloys that are difficult to produce as single crystals because of the intrinsic processing difficulty but also to the lack of industrial interest. Our simulations deal with ideal single crystal laminates and simulations for polycrystals remain to be done. However, as shown by the two-dimensional strain gradient plasticity simulations performed by Ohno and Okumura (2008) based on the rank-one potential the effect pertains for polycrystals. However these authors did not recognize the physical reality of the simulated phenomena. Instead they further developed the model to replace the rank one energy potential by a dissipative formulation which leads to fatigue loops without inflection points.

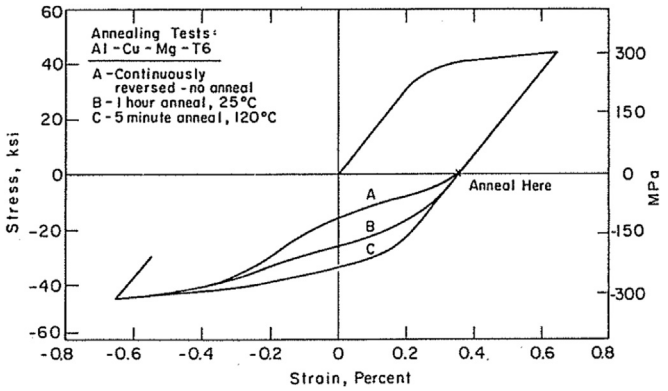

Fig. 11. Interrupted annealing hysteresis curves for an Al–Cu–Mg–T6 alloy tested at room temperature: A—continuously reverse load (no anneal), B—annealed 1 h/25 °C and C—annealed 5 min/120 °C, after Stoltz and Pelloux (1976).

4. Numerical solution aspects

The numerical solution strategy is formulated for the general three-dimensional case. For the laminate problem, the implementation can be simplified in a straightforward way.

4.1. Incremental potential

It is convenient to introduce slip parameters $\hat{\lambda} = (\lambda_1, \lambda_2, \ldots, \lambda_{2N})^{\mathrm{T}}$ for the numerical implementation, where N is the number of slip systems. Two slip parameters per slip system are introduced which account for positive and negative slip increments separately. These are associated to the positive and negative slip directions $\boldsymbol{d}_\alpha$ and $-\boldsymbol{d}_\alpha$, i.e., the total slip γ_α of a given slip system is represented by the difference of the associated two slip parameters. As a consequence, the flow rule (20) is replaced by

$$\dot{\lambda}_\alpha = \dot{\gamma}_0 \left\langle \frac{\tau_\alpha^{\mathrm{eff}} - (\tau^{\mathrm{C}} + q)}{\tau^{\mathrm{D}}} \right\rangle^p, \tag{61}$$

where, for simplicity, it is assumed that γ_{eq} is the only history variable, i.e. $\hat{\nu} = (\gamma_{\mathrm{eq}})$.

The numerical solution is based on the implicit Euler scheme. This means that the time is discretized into steps. Quantities of the preceding time step are marked by an index "n". For convenience, the index "$n+1$" is dropped. Increments are marked by the symbol "Δ".

Subsequently, it will be discussed that the overall problem can be reformulated as the stationarity conditions of the following potential:

$$\Pi = \Pi_{\mathrm{W}} + \Pi_{\mathrm{L}} + \Pi_{\mathcal{D}} + \Pi_{\mathrm{ext}}, \tag{62}$$

with a contribution from the free energy

$$\Pi_{\mathrm{W}} = \int_{\mathcal{B}} \left(W_{\mathrm{e}}(\mathrm{sym}(\nabla \boldsymbol{u}), \boldsymbol{\varepsilon}^{\mathrm{p}}(\hat{\lambda})) + W_{\mathrm{g}}(\boldsymbol{\alpha}) + W_{\mathrm{h}}(\gamma_{\mathrm{eq}}(\hat{\lambda})) \right) \mathrm{d}v, \tag{63}$$

a Lagrange-contribution

$$\Pi_{\mathrm{L}} = \int_{\mathcal{B}} \left(\boldsymbol{s} \cdot \left(\boldsymbol{H}^{\mathrm{p}} - \sum_\alpha \lambda_\alpha \boldsymbol{d}_\alpha \otimes \boldsymbol{n}_\alpha \right) + \boldsymbol{M} \cdot \left(\mathrm{curl}^{\mathrm{T}}(\boldsymbol{H}^{\mathrm{p}}) - \boldsymbol{\alpha} \right) \right) \mathrm{d}v, \tag{64}$$

a dissipative contribution

$$\Pi_{\mathcal{D}} = \int_{\mathcal{B}} \Delta t \left(\sum_\alpha \tau_\alpha^{\mathrm{d}} \frac{\Delta \lambda_\alpha}{\Delta t} - \frac{\dot{\gamma}_0 \, \tau^{\mathrm{D}}}{p+1} \left\langle \frac{\tau_\alpha^{\mathrm{d}} - \tau^{\mathrm{C}}}{\tau^{\mathrm{D}}} \right\rangle^{p+1} \right) \mathrm{d}v \tag{65}$$

and an external force contribution

$$\Pi_{\mathrm{ext}} = -\int_{\partial \mathcal{B}_t} \bar{\boldsymbol{t}} \cdot \boldsymbol{u} \, \mathrm{d}a - \int_{\partial \mathcal{B}_m} \bar{\boldsymbol{m}} \cdot \boldsymbol{H}^{\mathrm{p}} \, \mathrm{d}a. \tag{66}$$

The stationarity conditions associated to the potential Π with respect to the (a priori independent) arguments $\{\boldsymbol{u}, \boldsymbol{H}^{\mathrm{p}}, \hat{\lambda}, \boldsymbol{s}, \boldsymbol{M}, \boldsymbol{\alpha}, \hat{\tau}^{\mathrm{d}}\}$ yield the system equations. Here $\hat{\tau}^{\mathrm{d}} = (\tau_1^{\mathrm{d}}, \tau_2^{\mathrm{d}}, \ldots, \tau_{2N}^{\mathrm{d}})^{\mathrm{T}}$ can be interpreted as dissipative shear stresses. The principle of virtual power (Eq. (6)) is recovered by the conditions $\delta_{\boldsymbol{u}}\Pi = 0$ and $\delta_{\boldsymbol{H}^{\mathrm{p}}}\Pi = 0$. Note that the relations $\boldsymbol{\sigma} = \partial_{\boldsymbol{\varepsilon}} W_{\mathrm{e}}$ with $\boldsymbol{\varepsilon} = \mathrm{sym}(\nabla \boldsymbol{u})$ are implicitly accounted for. Eqs. (2) and (11) are obtained by $\delta_{\boldsymbol{M}}\Pi = 0$ and $\delta_{\boldsymbol{s}}\Pi = 0$, respectively. These relations illustrate the interpretation of the stresses $\boldsymbol{M}$ and $\boldsymbol{s}$ as Lagrange multipliers which enforce the kinematic relations (2) and (11).

Evaluation of the condition $\delta_{\boldsymbol{\alpha}}\Pi = 0$ yields the relation $\boldsymbol{M} = \partial_{\boldsymbol{\alpha}} W_{\mathrm{g}}$. Finally, the conditions $\delta_{\lambda_\alpha}\Pi = 0$ and $\delta_{\tau_\alpha^{\mathrm{d}}}\Pi = 0$ yield in combination the implicit Euler scheme associated to the flow rule

$$\frac{\Delta\lambda_\alpha}{\Delta t} = \dot{\gamma}_0 \left\langle \frac{\tau_\alpha^{\mathrm{eff}} - (\tau^{\mathrm{C}} + q)}{\tau^{\mathrm{D}}} \right\rangle^p, \tag{67}$$

with $\tau_\alpha^{\mathrm{eff}} = (\partial_{\boldsymbol{\varepsilon}} W + \boldsymbol{s})\cdot(\boldsymbol{d}_\alpha \otimes \boldsymbol{n}_\alpha)$ and $\boldsymbol{\varepsilon} = \mathrm{sym}(\nabla \boldsymbol{u})$.

4.2. Augmented Lagrange multiplier and penalty method

The augmented Lagrange multiplier method is based on the replacement of the Lagrange multipliers $\boldsymbol{M}$ and $\boldsymbol{s}$ in Eq. (64) by

$$\boldsymbol{M} = \boldsymbol{M}^{\mathrm{old}} + H_\chi^{\mathrm{M}}(\mathrm{curl}^{\mathrm{T}}(\boldsymbol{H}^{\mathrm{p}}) - \boldsymbol{\alpha}), \tag{68}$$

$$\boldsymbol{s} = \boldsymbol{s}^{\mathrm{old}} + H_\chi^{\mathrm{s}}\left(\boldsymbol{H}^{\mathrm{p}} - \sum_\alpha \lambda_\alpha \boldsymbol{d}_\alpha \otimes \boldsymbol{n}_\alpha\right). \tag{69}$$

Here, H_χ^{M} and H_χ^{s} are penalty parameters and $\boldsymbol{M}^{\mathrm{old}}$ as well as $\boldsymbol{s}^{\mathrm{old}}$ are approximations of the actual Lagrange multipliers. As a consequence of the replacements (68) and (69), the set of arguments of the potential Π (Eq. (62)) reduces to $\{\boldsymbol{u}, \boldsymbol{H}^{\mathrm{p}}, \hat{\lambda}, \boldsymbol{\alpha}, \hat{\tau}^{\mathrm{d}}\}$. Once a converged solution has been obtained (i.e. the stationarity conditions are satisfied), the following update is effectuated:

$$\boldsymbol{M}^{\mathrm{old}} \leftarrow \boldsymbol{M}^{\mathrm{old}} + H_\chi^{\mathrm{M}}(\mathrm{curl}^{\mathrm{T}}(\boldsymbol{H}^{\mathrm{p}}) - \boldsymbol{\alpha}), \tag{70}$$

$$\boldsymbol{s}^{\mathrm{old}} \leftarrow \boldsymbol{s}^{\mathrm{old}} + H_\chi^{\mathrm{s}}\left(\boldsymbol{H}^{\mathrm{p}} - \sum_\alpha \lambda_\alpha \boldsymbol{d}_\alpha \otimes \boldsymbol{n}_\alpha\right) \tag{71}$$

and the computation of the solution is repeated with an updated set of Lagrange multipliers yielding an improved approximation of Eqs. (2) and (11). The overall procedure is reiterated until Eqs. (2) and (11) are satisfied up to a certain tolerance.

If H_χ^{M} and H_χ^{s} are very large, the solution might be sufficiently accurate after one iteration already. In this case, the updates (70) and (71) are dispensable and can be omitted. Then, the scheme represents a penalty method (which has been used to obtain the numerical results in the work at hand with $H_\chi^{\mathrm{M}} = H_\chi^{\mathrm{s}} = 10^6$ MPa). Note that, in contrast to the original model (21), $\boldsymbol{M}$ can be computed even if $\boldsymbol{\alpha} = \boldsymbol{0}$. The close connection to classical elasto-plasticity will become obvious during the subsequent discussion of the local Algorithm 2.

4.3. Local algorithms

The principle of virtual power (6) is discretized by the finite element method. At the integration points, the following two algorithms allow the determination of the stresses.

Algorithm 1. Compute the stresses $\{\boldsymbol{\sigma}, \boldsymbol{s}, q\}$ by solving the nonlinear system of equations:

$$\boldsymbol{0} = -\mathbb{S}[\boldsymbol{\sigma}] + \boldsymbol{\varepsilon} - \boldsymbol{\varepsilon}_{\mathrm{n}}^{\mathrm{p}} - \sum_\alpha \Delta\mathbf{t}\dot{\gamma}_0 \left\langle \frac{(\boldsymbol{\sigma} + \boldsymbol{s})\cdot(\boldsymbol{d}_\alpha \otimes \boldsymbol{n}_\alpha) - \mathbf{q} - \tau^{\mathrm{C}}}{\tau^{\mathrm{D}}} \right\rangle^p \mathrm{sym}(\boldsymbol{d}_\alpha \otimes \boldsymbol{n}_\alpha)$$

$$\frac{\boldsymbol{s}}{H_\chi^{\mathrm{s}}} = \frac{\boldsymbol{s}^{\mathrm{old}}}{H_\chi^{\mathrm{s}}} + \boldsymbol{H}^{\mathrm{p}} - \sum_\alpha \left(\lambda_{\alpha,n} + \Delta t\dot{\gamma}_0 \left\langle \frac{(\boldsymbol{\sigma} + \boldsymbol{s})\cdot(\boldsymbol{d}_\alpha \otimes \boldsymbol{n}_\alpha) - q - \tau^{\mathrm{C}}}{\tau^{\mathrm{D}}} \right\rangle^p \right) \boldsymbol{d}_\alpha \otimes \boldsymbol{n}_\alpha$$

$$0 = q - \partial_{\gamma_{\mathrm{eq}}} W_{\mathrm{h}}.$$

Here, $\mathbb{S} = \mathbb{C}^{-1}$ denotes the compliance tensor. The linearization of this system of equations yields the consistent linearizations (tangent operators) of the stresses $\{\boldsymbol{\sigma}, \boldsymbol{s}, q\}$ (for details see, e.g., Wulfinghoff et al., 2013b, for a similar problem).

Algorithm 2. The following non-smooth energy is considered:

$$W_g = cGb \parallel \boldsymbol{\alpha} \parallel + W_g^s(\parallel \boldsymbol{\alpha} \parallel), \tag{72}$$

where $W_g^s = W_g^s(\parallel \boldsymbol{\alpha} \parallel)$ is assumed to be convex and smooth. For simplicity, it is assumed that $W_g^s = El_s^2 \parallel \boldsymbol{\alpha} \parallel^2/2$. Then the following algorithm can be applied.

Trial step: Set $\tilde{\boldsymbol{\alpha}} = \mathrm{curl}^T(\boldsymbol{H}^p)$

$$\boldsymbol{\alpha}^{Tr} = \boldsymbol{0}, \quad \boldsymbol{M}^{Tr} = \boldsymbol{M}^{old} + H_\chi^M(\tilde{\boldsymbol{\alpha}} - \boldsymbol{\alpha}^{Tr}), \quad \varphi^{Tr} = \parallel \boldsymbol{M}^{Tr} \parallel - cGb. \tag{73}$$

If $\varphi^{Tr} \leq 0$

$$\boldsymbol{\alpha} = \boldsymbol{\alpha}^{Tr} = \boldsymbol{0}, \quad \boldsymbol{M} = \boldsymbol{M}^{Tr} \tag{74}$$

else set

$$\boldsymbol{N}^{Tr} = \frac{\boldsymbol{M}^{Tr}}{\parallel \boldsymbol{M}^{Tr} \parallel}, \quad \boldsymbol{\alpha} = \frac{\varphi^{Tr}}{H_\chi^M + El_s^2}\boldsymbol{N}^{Tr}, \quad \boldsymbol{M} = \boldsymbol{M}^{Tr} - H_\chi^M \boldsymbol{\alpha}. \tag{75}$$

For the FE-implementation, the linearization of $\boldsymbol{M}$ w.r.t. $\tilde{\boldsymbol{\alpha}}$ can be obtained by the linearization of the algorithm.

Note the formal similarity of Algorithm 2 and classical radial-return algorithms (e.g.. Simo and Hughes, 1998).

In the work at hand, a linear-viscous model ($p = 1$) with very small viscosity ($\dot{\gamma}_0 = 10^3\ \mathrm{s}^{-1}$, $\tau^D = 1$ MPa) has been applied. The total simulation time was 1 s. The penalty approximation (70) (with $\boldsymbol{M}^{old} = \boldsymbol{0}$) has only been used for the rank-one potential. This is not necessary for the regularized logarithmic energy (57), which is smooth. The problem has been solved using 50 one-dimensional linear elements. The results correspond to Figs. 4, 5 and 9 in Section 3.

5. Summary

The novel aspects presented in this work are the analytical and numerical solutions of the problem of monotonic and cyclic shearing of laminate microstructures within the framework of strain gradient plasticity. An unusual type of kinematic hardening characterized by hysteresis loops with inflections is predicted and compared to experimental evidence from the literature, showing the physical relevance of the derived properties. The solutions have been derived analytically and numerically for strain gradient plasticity material laws based on two different defect energies: a rank-one and a logarithmic energy. The logarithmic energy leads to a backstress, the internal length scale of which is determined by the GND-density. A regularization of the non-convex logarithmic energy has been discussed. The regularized energy turns out to allow for a physical interpretation. Under certain conditions, the model can be interpreted as a gradient plasticity approximation of the theory of Groma et al. (2003).

We have shown that the overall yield stress of the rank-one problem is size dependent, while the hardening is not. The yield stress increase scales inversely with the size. The dislocation pile-ups degenerate into singular dislocation walls at the boundaries. The plastic slip and the backstress are constant inside the soft phase.

A significant new result provided in this work is that the logarithmic energy leads to a similar scaling of the 0.2%-offset yield stress, at least for the investigated model parameters, although the inverse scaling relation is not exactly met. The exact scaling is provided by an explicit analytical formula. The logarithmic model allows for non-homogeneous distribution of plastic slip and backstress in the channel and leads to hardening effects in addition to the yield stress increase. The predicted hardening is found to be only slightly influenced by the size.

The numerical implementation is discussed with focus on non-smooth defect energies like the rank-one potential. These non-smooth potentials can be described using sub-differentials. This implies that the generalized stresses can be computed from the dislocation density tensor uniquely only for non-vanishing values thereof. Sub-differentials are commonly applied in classical plasticity theory. Here, a sub-differential is equivalent to the introduction of an elastic range. Within this range, the Cauchy stress can be computed from the elastic strains. By analogy, this observation leads to a new regularization technique. This method allows for the computation of the generalized stresses, even for vanishing values of the dislocation density tensor.

A remarkable feature of the logarithmic model is that it provides a strain gradient plasticity based continuum description of Asaro's KIII nonlinear kinematic hardening mechanism associated with a perfect form of recovery of plastic memory. It represents a continuum model of the *first in/last out* scenario of dislocation motion under cyclic loading. At the microscale, cross-slip and interactions with forest dislocations are responsible for the partial loss of memory and explain why inflection points are very often not observed in experimental curves. Another origin of such a fading memory in a polycrystal is the interaction between grains. Computations of polycrystalline aggregates based on the proposed logarithmic potential therefore represent a necessary step for future research in this field, using the numerical scheme presented in this work. Similar hysteresis loops were obtained by Ohno and Okumura (2008) using the rank one model in two-dimensional simulations of polycrystalline aggregates. They were interpreted by the authors as an unusual Bauschinger effect, which prompted them to propose a new model formulation based on purely dissipative strain gradient plasticity effect. In contrast, we have shown in the present work overwhelming evidence in the literature of this effect in many alloys presenting a

population of nonshearable precipitates with homogeneous size distribution like iron or aluminium based alloys, up to nickel-base superalloys. The loops with inflections are observed only during the first to third cycles of the overall response of polycrystalline materials. This suggests that plasticity can be almost completely *reversed* at least at the early stages of plasticity. After the first cycles statistical effects associated with cross-slip and forest interaction do not allow for such reversibility any more. The evidence of such memory effects in plasticity confirms the idea that energy can be stored and released based on the dislocation density tensor and that the rank 1, and, preferably, the logarithmic formulation provide a relevant phenomenological descriptions of this property.

The proposed models illustrated in the case of ideal laminate and single slip situations must be complemented by additional isotropic hardening contributions coming from dislocation forest interaction but also probably by dissipative phenomena associated with the dislocation density tensor as suggested by Ohno and Okumura (2008).

One of the properties of the logarithmic defect energy that is being advocated is its nonconvexity. Obviously, non-convexity may have physical grounds and there is no obvious reason to discard it. Note that the analytical solution with the logarithmic potential was obtained in the absence of regularization but we have not investigated its stability. The scaling law for the size dependent yield stress is evaluated at a given fixed amount of plastic strain, typically 0.2%, in the convex branch of the model with the parameters chosen. The proposed regularization aims at restoring the differentiability at zero GND content. It is used for the numerical simulation and is motivated by the competition between densities of GND and SSD predominating at the beginning of plastic flow in the laminate. For the analytical solution, an initial GND density value is introduced and the material remains in the convex region of the potential during shearing. The non-convex part in the absence of an initial GND density indeed deserves further study and may require additional regularization by higher order gradients.

Finally, the formulation based on the dislocation density tensor alone instead of individual GND densities is a useful pragmatic choice that allows for efficient finite element computations. However it may exhibit some limitations to be explored in the context of multislip, as attempted for instance by Bardella et al. (2013).

Acknowledgments

The authors acknowledge the support rendered by the German Research Foundation (DFG) under Grant BO 1466/5-1. The funded project “Dislocation based Gradient Plasticity Theory” is part of the DFG Research Group 1650 “Dislocation based Plasticity”.

Appendix A. Vanishing external power of microtractions

The second term of Eq. (39) reads

$$\int_{\Delta\mathcal{B}} \boldsymbol{m}\cdot\dot{\boldsymbol{H}}^{\mathrm{p}}\,\mathrm{d}a, \tag{76}$$

with $\dot{\boldsymbol{H}}^{\mathrm{p}} = \dot{\gamma}\boldsymbol{e}_1 \otimes \boldsymbol{e}_2$ and

$$\boldsymbol{m} \overset{(8)}{=} \boldsymbol{M}\hat{\boldsymbol{n}}. \tag{77}$$

The boundary is given by $\partial(\Delta\mathcal{B}) = A_1^+ \cup A_1^- \cup A_2^+ \cup A_2^- \cup A_3^+ \cup A_3^-$, where $A_i^{\pm}$ denote the surfaces of the cuboid $\Delta\mathcal{B}$ with associated surface normals $\boldsymbol{e}_i^{\pm}$ ($i = 1, 2, 3$). At the top and bottom ($A_2^{\pm}$), the microtractions read

$$\boldsymbol{m}_{\mathrm{T}} = \boldsymbol{M}(x_1)\hat{\boldsymbol{n}}_{\mathrm{T}}, \quad \hat{\boldsymbol{n}}_{\mathrm{T}} \overset{(9)}{=} -\epsilon\boldsymbol{e}_2 = -\hat{\boldsymbol{n}}_{\mathrm{B}} \tag{78}$$

$$\Rightarrow \boldsymbol{m}_{\mathrm{B}} = \boldsymbol{M}(x_1)\hat{\boldsymbol{n}}_{\mathrm{B}} = -\boldsymbol{m}_{\mathrm{T}}. \tag{79}$$

Since $\dot{\boldsymbol{H}}_{\mathrm{T}}^{\mathrm{p}} = \dot{\boldsymbol{H}}_{\mathrm{B}}^{\mathrm{p}}$, the top and bottom contributions ($A_2^{\pm}$) to the integral (76) cancel each other. The $A_3^{\pm}$-contributions vanish based on analogous arguments. The $A_1^{\pm}$-contributions vanish since $\dot{\boldsymbol{H}}^{\mathrm{p}} = \boldsymbol{0}$ in the elastic phase.

Appendix B. Power balance for rank-one energy

With the representation $W = W_{\mathrm{e}} + W_{\mathrm{g}}$ (Eq. (13)), the power of internal forces (41) can be rewritten as

$$\mathcal{P}_{\mathrm{int}}(\Delta\mathcal{B}) = \int_{\Delta\mathcal{B}} \left(\partial_{\boldsymbol{\epsilon}} W_{\mathrm{e}}\cdot\dot{\boldsymbol{\epsilon}} + \partial_{\boldsymbol{\epsilon}^{\mathrm{p}}} W_{\mathrm{e}}\cdot\dot{\boldsymbol{\epsilon}}^{\mathrm{p}} + \dot{W}_{\mathrm{g}} + \mathcal{D}\right)\mathrm{d}v. \tag{80}$$

Since $W_{\mathrm{e}} = (\boldsymbol{\epsilon} - \boldsymbol{\epsilon}^{\mathrm{p}})\cdot\mathbb{C}[\boldsymbol{\epsilon} - \boldsymbol{\epsilon}^{\mathrm{p}}]/2$, it follows that $\boldsymbol{\sigma} = \partial_{\boldsymbol{\epsilon}} W_{\mathrm{e}} = -\partial_{\boldsymbol{\epsilon}^{\mathrm{p}}} W_{\mathrm{e}}$ and

$$\mathcal{P}_{\text{int}}(\Delta\mathcal{B}) = \int_{\Delta\mathcal{B}} \left(\boldsymbol{\sigma}\cdot\dot{\boldsymbol{e}} - \boldsymbol{\sigma}\cdot(\dot{\gamma}\ \text{sym}(\boldsymbol{e}_1 \otimes \boldsymbol{e}_2)) + \dot{W}_{\text{g}} + (\tau^{\text{C}} + \tau^{\text{D}}\dot{\gamma}/\dot{\gamma}_0)\dot{\gamma} \right) \text{d}v. \tag{81}$$

Here, Eq. (37) has been applied. From $\mathcal{P}_{\text{ext}}(\Delta\mathcal{B}) = \mathcal{P}_{\text{int}}(\Delta\mathcal{B})$ and Eq. (40), it follows that

$$\int_{-s/2-\epsilon}^{s/2+\epsilon} \left(-\sigma_{12}\,\dot{\gamma} + \dot{W}_{\text{g}} + \left(\tau^{\text{C}} + \tau^{\text{D}}\frac{\dot{\gamma}}{\dot{\gamma}_0} \right)\dot{\gamma} \right) \text{d}x_1 = 0. \tag{82}$$

The total defect energy rate is given by

$$\int_{-s/2-\epsilon}^{s/2+\epsilon} \dot{W}_{\text{g}}\ \text{d}x_1 \overset{(33)}{=} cGb\,\frac{\text{d}}{\text{d}t} \int_{-s/2-\epsilon}^{s/2+\epsilon} |\gamma'(x_1)|\ \text{d}x_1 \tag{83}$$

$$\int_{-s/2-\epsilon}^{s/2+\epsilon} \dot{W}_{\text{g}}\ \text{d}x_1 \overset{(38)}{=} cGb\,\frac{\text{d}}{\text{d}t} \int_{-s/2-\epsilon}^{0} \gamma'(x_1)\ \text{d}x_1 - cGb\,\frac{\text{d}}{\text{d}t} \int_{0}^{s/2+\epsilon} \gamma'(x_1)\ \text{d}x_1 \tag{84}$$

$$\int_{-s/2-\epsilon}^{s/2+\epsilon} \dot{W}_{\text{g}}\ \text{d}x_1 = 2cGb\,\dot{\gamma}(0). \tag{85}$$

From this equation and Eq. (82), relation (42) immediately follows.

Appendix C. Sensitivity analysis

According to Eq. (56) the macroscopic shear strain can be additively decomposed into an elastic part σ_{12}/G and a plastic part

$$\bar{\gamma}_{\text{p}}/\alpha_0 = \frac{L}{e(s+h)} \left(\exp\left(\frac{s}{2L}\right)(s-2L) + 2L \right), \tag{86}$$

with L as defined in Eq. (55). The stress can be obtained as the inverse of (86), $\sigma_{12} = g(\bar{\gamma}_{\text{p}}/\alpha_0)$. The function g is illustrated qualitatively in Fig. 12.

The total differential reads

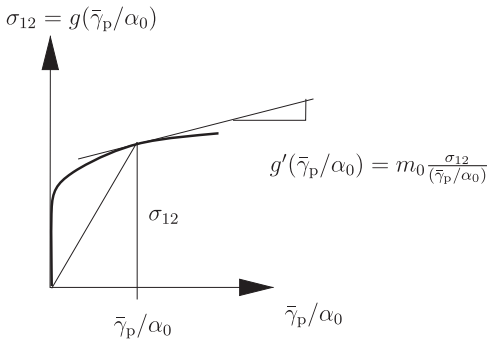

Fig. 12. Visualization of the function $g(\bar{\gamma}_{\text{p}}/\alpha_0)$.

$$\text{d}\sigma_{12} = \partial_{\bar{\gamma}\text{p}}\sigma_{12}\ \text{d}\bar{\gamma}_{\text{p}} + \partial_{\alpha 0}\sigma_{12}\ \text{d}\alpha_0 = g'\ \text{d}\left(\frac{\bar{\gamma}_{\text{p}}}{\alpha_0}\right) \tag{87}$$

$$\text{d}\sigma_{12} = \frac{1}{\alpha_0} g'\ \text{d}\bar{\gamma}_{\text{p}} - \frac{\bar{\gamma}_{\text{p}}}{\alpha_0^2} g'\ \text{d}\alpha_0. \tag{88}$$

Hence, the sensitivity of σ_{12} with respect to changes of α_0 reads

$$\partial_{\alpha 0}\,\sigma_{12} = -\frac{\bar{\gamma}_{\text{p}}}{\alpha_0^2} g'. \tag{89}$$

In the region of well-established plastic flow, one might conclude from Fig. 12 that

$$\partial_{\alpha 0}\,\sigma_{12} = -\frac{\bar{\gamma}_p}{\alpha_0^2} g' = -\,m_0 \frac{\bar{\gamma}_p}{\alpha_0^2}\frac{\sigma_{12}}{(\bar{\gamma}_p/\alpha_0)} = -\,m_0 \frac{\sigma_{12}}{\alpha_0}, \tag{90}$$

where m_0 takes a small value <1. At constant plastic strain, small variations of α_0 lead to the following variations of σ_{12}:

$$\Delta\sigma_{12} \approx -\,\sigma_{12}\, m_0 \frac{\Delta\alpha_0}{\alpha_0}. \tag{91}$$

Since m_0 is expected to be small, variations $|\Delta\alpha_0| < \alpha_0$ have a small influence on the overall size effect.

References

Aifantis, E.C., 1987. The physics of plastic deformation. Int. J. Plast. 3 (3), 211–247.
Asaro, R.J., 1975. Elastic–plastic memory and kinematic hardening. Acta Metall. 23, 1255–1265.
Ashby, M., 1970. The deformation of plastically non-homogeneous materials. Philos. Mag. 21 (170), 399–424.
Aslan, O., Cordero, N.M., Gaubert, A., Forest, S., 2011. Micromorphic approach to single crystal plasticity and damage. Int. J. Eng. Sci. 49, 1311–1325.
Bardella, L., Segurado, J., Panteghini, A., Llorca, J., 2013. Latent hardening size effects in small-scale plasticity. Model. Simul. Mater. Sci. Eng. 21, 055009.
Berdichevsky, V., 2006. On thermodynamics of crystal plasticity. Scr. Mater. 54, 711–716.
Boehler, J., 1977. On irreducible representations for isotropic scalar functions. Z. Angew. Math. Mech. 57, 323–327.
Conti, S., Ortiz, M., 2005. Dislocation microstructures and the effective behavior of single crystals. Arch. Ration. Mech. Anal. 176, 103–147.
Cordero, N.M., Forest, S., Busso, E., Berbenni, S., Cherkaoui, M., 2012. Grain size effects on plastic strain and dislocation density tensor fields in metal polycrystals. Comput. Mater. Sci. 52, 7–13.
Cordero, N.M., Gaubert, A., Forest, S., Busso, E., Gallerneau, F., Kruch, S., 2010. Size effects in generalised continuum crystal plasticity for two-phase laminates. J. Mech. Phys. Solids 58, 1963–1994.
De Luca, L., Garroni, A., Ponsiglione, M., 2012. Gamma-convergence analysis of systems of edge dislocations: the self energy regime. Arch. Ration. Mech. Anal. 206, 885–910.
Forest, S., 2008. Some links between Cosserat, strain gradient crystal plasticity and the statistical theory of dislocations. Philos. Mag. 88, 3549–3563.
Forest, S., 2009. Micromorphic approach for gradient elasticity, viscoplasticity, and damage. J. Eng. Mech. 135, 117–131.
Forest, S., Guéninchault, N., 2013. Inspection of free energy functions in gradient crystal plasticity. Acta Mech. Sin., 29 (6), 763-772.
Forest, S., Sedláček, R., 2003. Plastic slip distribution in two-phase laminate microstructures: dislocation-based vs. generalized-continuum approaches. Philos. Mag. A 83, 245–276.
Geers, M., Peerlings, R., Peletier, M., Scardia, L., 2013. Asymptotic behaviour of a pile-up of infinite walls of edge dislocations. Arch. Ration. Mech. Anal. 209, 495–539.
Groma, I., Csikor, F., Zaiser, M., 2003. Spatial correlations and higher-order gradient terms in a continuum description of dislocation dynamics. Acta Mater. 51 (5), 1271–1281.
Groma, I., Györgyi, G., Kocsis, B., 2007. Dynamics of coarse grain grained dislocation densities from an effective free energy. Philos. Mag. 87, 1185–1199.
Gruber, P.A., Böhm, J., Onuseit, F., Wanner, A., Spolenak, R., Arzt, E., 2008. Size effects on yield strength and strain hardening for ultra-thin Cu films with and without passivation: a study by synchrotron and bulge test techniques. Acta Mater. 56, 2318–2335.
Gurtin, M.E., Anand, L., Lele, S.P., 2007. Gradient single-crystal plasticity with free energy dependent on dislocation densities. J. Mech. Phys. Solids 55, 1853–1878.
Hall, E.O., 1951. The deformation and aging of mild steel. Part III: discussion and results. Proc. Phys. Soc. Lond. 64, 747–753.
Han, W., Reddy, B., 2013. Plasticity: Mathematical Theory and Numerical Analysis. Springer, New York.
Hurtado, D.E., Ortiz, M., 2012. Surface effects and the size-dependent hardening and strengthening of nickel micropillars. J. Mech. Phys. Solids 60 (8), 1432–1446.
Hurtado, D.E., Ortiz, M., 2013. Finite element analysis of geometrically necessary dislocations in crystal plasticity. Int. J. Numer. Methods Eng. 93 (1), 66–79.
Kametani, R., Kodera, K., Okumura, D., Ohno, N., 2012. Implicit iterative finite element scheme for a strain gradient crystal plasticity model based on self-energy of geometrically necessary dislocations. Comput. Mater. Sci. 53 (1), 53–59.
Kröner, E., 1958. Kontinuumstheorie der Versetzungen und Eigenspannungen. Springer-Verlag, Berlin.
Mesarovic, S.D., Baskaran, R., Panchenko, A., 2010. Thermodynamic coarsening of dislocation mechanics and the size-dependent continuum crystal plasticity. J. Mech. Phys. Solids 58 (3), 311–329.
Miehe, C., 2011. A multi-field incremental variational framework for gradient-extended standard dissipative solids. J. Mech. Phys. Solids 59, 898–923.
Mesarovic, S.D., Forest, S., Jaric, JP., 2015. Size-dependent energy in crystal plasticity and continuum dislocation models. Proc. R. Soc. A 471, 20140868, http://dx.doi.org/10.1098/rspa.2014.0868.
Miehe, C., Mauthe, S., Hildebrand, F., 2013. Variational gradient plasticity at finite strains. Part iii: local–global updates and regularization techniques in multiplicative plasticity for single crystals. Comput. Methods Appl. Mech. Eng..
Nye, J.F., 1953. Some geometrical relations in dislocated crystals. Acta Metall. 1, 153–162.
Ohno, N., Okumura, D., 2007. Higher-order stress and grain size effects due to self energy of geometrically necessary dislocations. J. Mech. Phys. Solids 55, 1879–1898.
Ohno, N., Okumura, D., 2008. Grain-size dependent yield behavior under loading, unloading and reverse loading. Int. J. Mod. Phys. B 22, 5937–5942.
Ortiz, M., Repetto, E., 1999. Nonconvex energy minimization and dislocation structures in ductile single crystals. J. Mech. Phys. Solids 47 (2), 397–462.
Ortiz, M., Repetto, E., Stainier, L., 2000. A theory of subgrain dislocation structures. J. Mech. Phys. Solids 48 (10), 2077–2114.
Petch, N.J., 1953. The cleavage strength of polycrystals. J. Iron Steel Inst. 174, 25–28.
Proudhon, H., Poole, W., Wang, X., Bréchet, Y., 2008. The role of internal stresses on the plastic deformation of the Al–Mg–Si–Cu alloy AA611. Philos. Mag. 88, 621–640.
Reddy, B.D., Wieners, C., Wohlmuth, B., 2012. Finite element analysis and algorithms for single-crystal strain-gradient plasticity. Int. J. Numer. Methods Eng. 90 (6), 784–804.
Simo, J.C., Hughes, T., 1998. Computational Inelasticity. Springer-Verlag, New York.
Steinmann, P., 1996. Views on multiplicative elastoplasticity and the continuum theory of dislocations. Int. J. Eng. Sci. 34, 1717–1735.
Stölken, J.S., Evans, A.G., 1998. A microbend test method for measuring the plasticity length scale. Acta Mater. 46, 5109–5115.
Stoltz, R., Pelloux, R., 1974. Cyclic deformation and Bauschinger effect in Al–Cu–Mg alloys. Scr. Metall. 8, 269–276.
Stoltz, R., Pelloux, R., 1976. The Bauschinger effect in precipitation strengthened aluminum alloys. Metall. Trans. 7A, 1295–1306.
Svendsen, B., Bargmann, S., 2010. On the continuum thermodynamic rate variational formulation of models for extended crystal plasticity at large deformation. J. Mech. Phys. Solids 58 (9), 1253–1271.

Taillard, R., Pineau, A., 1982. Room temperature tensile properties of Fe–19 wt% Cr alloys precipitation hardened by the intermetallic compound NiAl. Mater. Sci. Eng. 56, 219–231.
Wulfinghoff, S., Bayerschen, E., Böhlke, T., 2013a. A gradient plasticity grain boundary yield theory. Int. J. Plast. 51, 33–46.
Wulfinghoff, S., Bayerschen, E., Böhlke, T., 2013b. Micromechanical simulation of the Hall–Petch effect with a crystal gradient theory including a grain boundary yield criterion. Proc. Appl. Math. Mech. 13, 15–18.
Wulfinghoff, S., Böhlke, T., 2012. Equivalent plastic strain gradient enhancement of single crystal plasticity: theory and numerics. Proc. R. Soc. A: Math. Phys. Eng. Sci. 468 (2145), 2682–2703.
Xiang, Y., Vlassak, J., 2006. Bauschinger and size effects in thin-film plasticity. Acta Mater. 54, 5449–5460.